blood advances®

PML-controlled responses in severe congenital neutropenia with *ELANE*-misfolding mutations

Patricia A. Olofsen,[1] Dennis A. Bosch,[1,*] Onno Roovers,[1,*] Paulina M. H. van Strien,[1,*] Hans W. J. de Looper,[1] Remco M. Hoogenboezem,[1] Sander Barnhoorn,[2] Pier G. Mastroberardino,[2] Mehrnaz Ghazvini,[3] Vincent H. J. van der Velden,[4] Eric M. J. Bindels,[1] Emma M. de Pater,[1] and Ivo P. Touw[1]

[1]Department of Hematology, [2]Department of Molecular Genetics, [3]Department of Developmental Biology, iPS Core Facility, and [4]Department of Immunology, Erasmus University Medical Center, Rotterdam, The Netherlands

Key Points

- PML reduces ROS but stimulates metabolism and ELANE expression in iPSC-derived CD34$^+$CD45$^+$ cells from *ELANE*-SCN with NE misfolding mutations.

- PML dampens granulocyte colony-stimulating factor responsiveness in a CSF3 therapy-refractory case of *ELANE*-SCN.

Mutations in *ELANE* cause severe congenital neutropenia (SCN), but how they affect neutrophil production and contribute to leukemia predisposition is unknown. Neutropenia is alleviated by CSF3 (granulocyte colony-stimulating factor) therapy in most cases, but dose requirements vary between patients. Here, we show that CD34$^+$CD45$^+$ hematopoietic progenitor cells (HPCs) derived from induced pluripotent stem cell lines from patients with SCN that have mutations in *ELANE* (n = 2) or *HAX1* (n = 1) display elevated levels of reactive oxygen species (ROS) relative to normal iPSC-derived HPCs. In patients with *ELANE* mutations causing misfolding of the neutrophil elastase (NE) protein, HPCs contained elevated numbers of promyelocyte leukemia protein nuclear bodies, a hallmark of acute oxidative stress. This was confirmed in primary bone marrow cells from 3 additional patients with *ELANE*-mutant SCN. Apart from responding to elevated ROS levels, PML controlled the metabolic state of these *ELANE*-mutant HPCs as well as the expression of *ELANE*, suggestive of a feed-forward mechanism of disease development. Both *PML* deletion and correction of the *ELANE* mutation restored CSF3 responses of these *ELANE*-mutant HPCs. These findings suggest that PML plays a crucial role in the disease course of *ELANE*-SCN characterized by NE misfolding, with potential implications for CSF3 therapy.

Introduction

Severe congenital neutropenia (SCN) is a genetically heterogeneous disease that, when left untreated, leads to life-threatening bacterial infections from the lack of neutrophils.[1] Autosomal dominant or sporadic mutations in *ELANE*, the gene encoding neutrophil elastase (NE), are the most frequent cause of SCN, whereas mutations in *HAX1*, encoding a multifunctional protein associated with mitochondrial integrity and cytoskeleton organization, are responsible for the autosomal recessive form of SCN originally described as Kostmann syndrome.[2,3] Most patients with SCN receive life-long therapy with colony-stimulating factor 3 (CSF3/granulocyte colony-stimulating factor [G-CSF]) to alleviate the neutrophilic differentiation block. Although the majority of patients respond favorably to relatively modest dosages of CSF3 (5-10 μg/kg per day), others need more excessive dosages (>50-100 μg/kg per day) to reach clinically beneficial neutrophil levels, whereas some patients fail to respond to CSF3 therapy altogether.[4] Patients with SCN have an increased risk of developing myelodysplastic syndrome (MDS) or acute myeloid leukemia (AML) while under CSF3 treatment. This particularly applies to patients needing high CSF3 dosages to alleviate neutropenia.[5,6]

How *ELANE*, *HAX1*, and other mutations causing SCN affect neutrophil production is still largely unknown. A prevailing hypothesis is that cellular stresses, in *ELANE*-SCN caused by NE protein misfolding and in *HAX1*-SCN by mitochondrial leakage, are drivers of the neutropenia.[3,7,8] However, the wide spectrum of *ELANE* mutations found in SCN are not all predicted to cause NE misfolding; therefore, alternative mechanisms of how *ELANE* mutations cause neutropenia have been proposed.[9-11] This heterogeneity of mutations may explain the variability in CSF3 responses seen in patients and possibly also determine leukemia risk.[4,5,9]

The promyelocytic leukemia protein (PML), originally identified as a fusion partner in a chromosomal translocation causing acute promyelocytic leukemia, has been studied extensively for its role in controlling cell cycle, DNA damage, and inflammation.[12-17] Particularly, these studies dealt with the role of PML nuclear bodies (PML-NBs), hollow spherical structures that contain a plethora of regulatory molecules controlling the previously mentioned processes. Moreover, PML-NBs have been implicated in degrading misfolded proteins by a mechanism not involving the canonical unfolded protein response (UPR) signaling pathways.[18] Finally, PML plays an important role in how cells deal with oxidative stress caused by reactive oxygen species (ROS).[19] Whereas nuclear factor erythroid 2-related factor 2 (NRF2) transcriptionally activates antioxidant pathways at relatively low levels of ROS, this role can be taken over by PML upon the acute generation of excess ROS (eg, induced by exposure of cells to arsenic trioxide [As_2O_3] or irradiation).[19]

To investigate the involvement of PML in SCN, we created patient- and control-derived induced pluripotent stem cells (iPSCs) and generated $CD34^+CD45^+$ hematopoietic progenitor cells (HPCs) from these lines. We show that PML-NBs are elevated in SCN-HPCs with predicted NE misfolding mutations and that PML deletion reduces the metabolic activity and partly restores CSF3 responses of these cells. In addition, we show that loss of PML reduces the levels of mutant *ELANE* transcript and NE protein, indicating that PML may aggravate the SCN phenotype through a feed-forward mechanism.

Materials and methods

Patient samples

Ficoll-gradient separated bone marrow (BM) and blood cells were obtained and frozen according to established procedures for viable cell cryopreservation. The study was performed under the permission of the institutional review boards of the Erasmus Medical Center.

Generation of iPSC

BM fibroblasts cultured from patients with SCN harboring *ELANE* mutation p.I60F (NC_000019.10:g.852986A>T), *ELANE* mutation p.R103L (NC_000019.10:g.853345G>T), or *HAX1* mutation p.W44X (NC_000001.11:g.154273412_154273413insA), and from a healthy control BM were reprogrammed, as described previously.[20] Cells were cultured in mTeSR1 (STEMCELL Technologies) on Geltrex LDEV-Free Reduced Growth Factor Basement Membrane Matrix (Thermo Fisher Scientific) and were regularly checked for pluripotency, correct karyotype and their ability to generate hematopoietic progenitor cells and mature neutrophils.

CRISPR/Cas9-mediated genome editing

CRISPR/Cas9-mediated genome editing was used to create $PML^{-/-}$ iPSCs, where a stop codon was introduced in exon 3, or correct the *ELANE*-I60F mutation. In short, 2×10^6 iPSCs were transfected by electroporation with 500 ng px330 (Cas9 plasmid, #42230 Addgene), containing a gene-specific guide RNA, and 1500 ng recombination template containing PML with a stop codon or *ELANE* wild-type sequence and a neomycin selection cassette, using the 4D-Nucleofector System (Lonza), program CA-137. G418 selection (50 μg/mL) started 48 hours after electroporation. Single clones were picked and screened for homozygous integration of the stop codon and absence of PML protein, or correct integration of the wild-type *ELANE* sequence in the *ELANE*-I60F mutant allele. All clones were checked for retainment of pluripotency.

Hematopoietic induction

HPCs ($CD34^+CD45^+$) were produced with the STEMdiff Hematopoietic Kit (STEMCELL Technologies) according to the manufacturer's protocol. Suspension cells were harvested at day 12 of the protocol and used for further downstream analysis.

Neutrophil differentiation

To expand myeloid progenitors and subsequently differentiate them into mature neutrophils, suspension cells, harvested at day 12 of the hematopoietic induction protocol, were treated as described previously.[21] In short, 10^5 cells/mL were plated in a nontissue culture-treated plate in Iscove modified Dulbecco medium (Life Technologies) complemented with 10% defined fetal bovine serum (Hyclone), 10 ng/mL interleukin 3 (IL-3; R&D Systems), 10 ng/mL granulocyte-macrophage colony-stimulating factor (Peprotech), 50 ng/mL stem cell factor (CellGenix GmbH), and 50 ng/mL CSF3 (Filgastrim; Zarzio). After 4 days, medium was switched to Iscove modified Dulbecco medium complemented with 10% defined fetal bovine serum and 50 ng/mL CSF3. Cells were harvested 5 days later and used for subsequent fluorescence-activated cell sorting (FACS) analysis with the EuroFlow AML tube 1, as described previously.[22,23]

Magnetic-activated cell sorting purification and immunofluorescence stainings

Suspension cells expressing CD45 were enriched using CD45 Microbeads (Miltenyi Biotec) and subsequent magnetic-activated cell sorting separation according to the manufacturer's protocol. Cells were attached to glass slides with Cytospin 4 and fixed in 4% paraformaldehyde (Polysciences) on ice for 20 minutes. Cells were washed with phosphate-buffered saline (PBS) and the primary antibodies (PML 1:1000, #M041-3 MBL, and NRF2 1:200, #ab31163 Abcam) were incubated overnight at 4°C in 0.05% Saponin (diluted in PBS; Merck). After washing 3 × 5 minutes in 0.05% Saponin, cells were incubated with the secondary antibodies (goat anti mouse Alexa Fluor 488, 1:200 Life or donkey anti rabbit Cy3 1:800, Bio-Connect) for 1 hour at 37°C. Cells were then washed 3 × 5 minutes in 0.05% Saponin and 2 × 5 minutes in PBS after which Hoechst 34580 (1:3000; Merck) was added for 10 minutes. Slides were mounted with ProLong Diamond Antifade Mountant (Merck) and imaged on a SP5 or SP8 confocal microscope (Leica). Quantifications were performed using Fiji software.[24]

Seahorse assay

The Agilent Seahorse XFe24 Cell Culture microplate (Agilent) was coated with 22.4 μg/mL Cell-Tak Cell and Tissue Adhesive (Corning) for 20 minutes at room temperature. Suspension cells, obtained after 12 days of hematopoietic induction, were harvested and subsequently live cells were sorted using 7AAD. Sorted live cells (1.25×10^5 per well) were added to the coated microplate and centrifuged for 5 minutes at 200g to form a monolayer of cells at the bottom of the well. Cell numbers and oligomycin, carbonyl cyanide-p-trifluoromethoxyphenylhydrazone, and antimycin concentrations (all 1.0 μM) were determined after optimization. Per condition, 5 wells were used for the Seahorse Mitochondrial Stress Test, which was performed according to the manufacturer's instructions and measured on a XFe24 analyzer. Data were analyzed with the Seahorse Wave Desktop Software (Agilent).

Colony-forming unit assays

ELANE-I60F patient BM cells (4×10^4/mL) or BM cells derived from a healthy control were seeded in triplicate for colony formation in methylcellulose (H4230, STEMCELL Technologies) with increasing concentrations of CSF3 (0, 1, 3.33, 10, 33.3, 100 ng/mL). Colonies were counted after 14 days of culture. A similar protocol was used for the iPSC-derived HPCs, where suspension cells were harvested after 12 days of hematopoietic differentiation and seeded (1×10^4/mL) in colony cultures with CSF3 concentrations as described previously.

RNA isolation and RNA sequencing

RNA was isolated from CD34$^+$CD45$^+$ HPCs using TRIzol (Thermo Fisher Scientific) and GenElute-LPA (Sigma-Aldrich) according to the manufacturer's protocol. Complementary DNA was generated with version 4 of the SMARTer Ultra Low Input RNA Kit for sequencing (Clontech). Sequencing libraries were generated using the TruSeq Nano DNA Sample Preparation Kit (Illumina), according to the low sample protocol and run on HiSeq 2500 or Novaseq 6000 instruments (Illumina).

Bioinformatics and statistics

Demultiplexing was performed using the CASAVA software (Illumina) allowing for 1 mismatch in the barcodes. Subsequently, SMARTer adapters and poly-A tails were removed (fqtrim; https://ccb.jhu.edu/software/fqtrim/) and quality metrics were estimated (FastQC, Babraham Bioinformatics and MultiQC; http://multiqc.info) for all of the resulting fastq files. Reads were then aligned against the Human Transcriptome (Gencode v19)/Genome (hg19) using the STAR aligner.[25] Abundance estimation was performed using Cufflinks (refSeq[26]), and raw counts were measured with the HTSeq-count software set in union mode.[27] Next, the measured raw counts were used to create clustering and principal component plots and to perform differential expression analysis using a combination of DESeq2[28] and R (https://www.r-project.org/). Finally, gene set enrichment analysis (GSEA) on the curated gene sets C2 and the hallmark pathways H was done using the GSEA software based on the preranked ASHR log$_2$ fold change, where a false discovery rate <0.05 was considered significant.[29,30] Transcripts per million (TPM) were calculated using StringTie.[31]

Quantification and statistical analysis

Data are presented as mean ± standard error of the mean. Comparison of 2 groups was performed using an unpaired Student t test. Statistical analyses were performed using GraphPad Prism 8.0 (GraphPad Software) or DESeq2. A value of $P < .05$ was considered significant.

Results

Elevated ROS levels and activation of the NRF2 antioxidant pathway in SCN-iPSC-derived HPCs

Both mutations in *ELANE* and *HAX1* have been reported to cause increased ROS levels in promyelocytes,[3,7,10,11,32] but whether more immature myeloid precursors of patients with SCN already experience oxidative stress because of elevated ROS has not previously been addressed. CellROX Deep Red analysis of HPCs derived from SCN-iPSCs with different mutations (*ELANE*-R103L [NC_000019.10:g.853345G>T], *ELANE*-I60F [NC_000019.10:g.852986A>T], and *HAX1*-W44X [NC_000001.11:g.154273412_154273413insA]) showed higher levels of ROS in SCN-HPCs compared with normal control HPCs (Figure 1A). Indicative of elevated ROS levels, NRF2, the master redox regulator,[33] was translocated to the nucleus and subsequently upregulated *GSR*, encoding the antioxidant enzyme glutathione reductase (Figure 1B-C).

Accumulation of PML-NBs in ELANE-SCN HPCs with predicted NE-misfolding mutations

PML-NBs are formed on acute generation of excessive oxidative stress to neutralize the effects of ROS that are not being coped with by the NRF2 antioxidant pathway.[19] Accordingly, the number of PML-NBs significantly increased after incubation of control HPCs with As$_2$O$_3$, which induces excessive oxidative stress (supplemental Figure 1A-B). In *ELANE*-I60F HPCs, higher numbers of PML-NBs were found relative to controls in the absence of As$_2$O$_3$, which was not seen in *ELANE*-R103L or *HAX1*-W44X HPCs (Figure 2A). Incubation with the antioxidant *N*-acetylcysteine significantly reduced ROS levels and the number of PML-NBs in *ELANE*-I60F cells, corroborating that in *ELANE*-I60F HPCs, PML-NBs were elevated by endogenous oxidative stress (supplemental Figure 1C-D). Comparison of the predicted structural alterations (https://www3.cmbi.umcn.nl/hope/)[34] caused by the *ELANE* mutations showed that the *ELANE*-R103L mutation alters a positively charged amino acid (R) into a smaller neutral amino acid (L) at the surface of the protein, thereby possibly affecting interactions with other molecules (Figure 2B). In contrast, the *ELANE*-I60F alteration causes a structural change in the core of the protein, by introducing a bulky amino acid, that predicts protein misfolding (Figure 2B). To exclude that the increased numbers of PML-NBs was a feature of iPSC-derived, rather than bona fide BM-derived HPCs, we quantified PML-NBs in CD34$^+$ cells from primary SCN BM samples. These analyses confirmed that PML-NBs are increased in *ELANE*-I60F HPCs relative to controls (Figure 2C). Importantly, this was also seen in HPCs from a second patient with SCN with a misfolding mutation (p.P139L NC_000019.10:g. 855614C>T), but not in HPCs from 2 patients with ELANE-SCN that have mutations (p.I120T NC_000019.10:g. 853396T>C, p.S204TfsX11 NC_000019.10:g. 855962_855969dup) not predicting NE misfolding (Figure 2D).

PML knockout induces NRF2 nuclear translocation in *ELANE*-I60F HPCs

Because NRF2 and PML-NBs both neutralize ROS levels, we wondered to what extent deletion of PML in the *ELANE*-I60F and
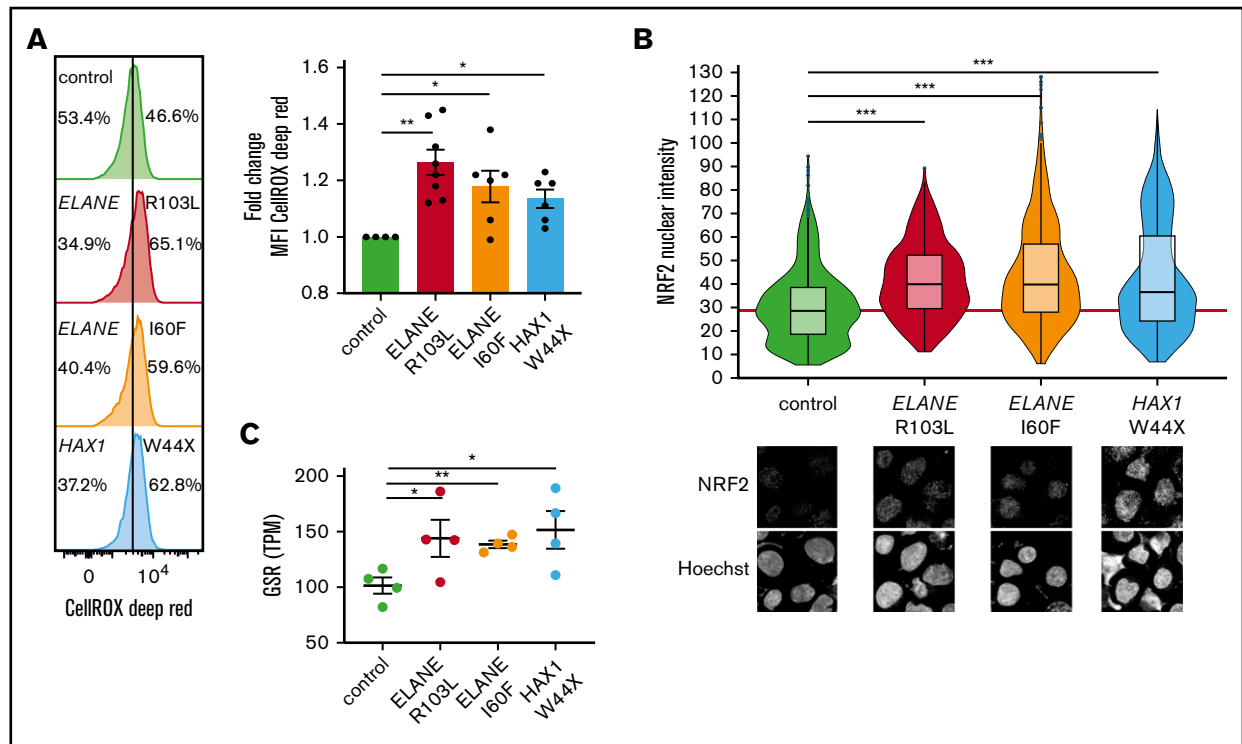
Figure 1. SCN-iPSC-derived CD34$^+$ CD45$^+$ cells show elevated ROS levels and increased nuclear translocation of NRF2. (A) Representative FACS histograms and quantifications of mean fluorescent intensities (MFI) showing increased levels of CellROX Deep Red in SCN HPCs. Data are from 3 independent experiments on 2 clones per genotype. (B) Quantification of the nuclear translocation of NRF2 by immunofluorescence stainings of HPCs showing increased nuclear NRF2 levels in SCN HPCs. The red line indicates the median NRF2 nuclear intensity for the control HPCs. Data are pooled from 2 independent clones and 5 independent experiments. Total cells analyzed: control, n = 765; *ELANE*-R103L, n = 721; *ELANE*-I60F, n = 677; *HAX1*-W44X, n = 574. (C) Expression of the antioxidant glutathione reductase (GSR) in TPM obtained from 2 different iPSC clones and 2 independent experiments. *$P < .05$, **$P < .01$, ***$P < .001$.

control HPCs affected NRF2 activation. Disruption of PML expression by introducing a stop codon in exon 3 (supplemental Figure 2A-B) resulted in the complete absence of PML-NBs (Figure 3A), but did not affect the generation of HPCs (supplemental Figure 2C-D). *ELANE*-I60F PML$^{-/-}$ HPCs showed significantly increased nuclear translocation of NRF2, confirming that PML-NBs reduced ROS levels, leading to lower NRF2 activation (Figure 3B). No major differences in total ROS levels were seen between PML proficient and deficient *ELANE*-I60F HPCs, indicating that NRF2, possibly in combination with other antioxidant pathways, compensated for the loss of PML (Figure 3C). In addition, As$_2$O$_3$ treatment of *ELANE*-R103L cells, which previously did not show increased numbers of PML-NBs but did show increased ROS levels and NRF2 translocation (Figures 1 and 2A), resulted in increased numbers of PML-NBs but not in increased ROS levels (supplemental Figure 1E-F), further strengthening the observation that both PML-NBs and NRF2 control ROS levels. No significant differences in nuclear NRF2 were seen between PML proficient and deficient control HPCs, consistent with earlier work showing that, under physiological ROS conditions, PML-NBs do not play a major role in governing antioxidant responses (Figure 3D).[19]

SCN mutations result in distinct transcriptional profiles in HPCs

To further study how *ELANE* and *HAX1* mutations affect cellular responses of HPCs, we performed RNA sequencing on FACS purified CD34$^+$CD45$^+$ cells derived from 2 different iPSC clones, stemming from 2 independent hematopoietic induction experiments for each genotype. Principal component analysis of these transcriptome data showed distinct clustering for each SCN subtype and controls (supplemental Figure 3A). The homozygous *HAX1*-W44X mutation is predicted to activate nonsense-mediated messenger RNA decay.[35] This was confirmed by GSEA, which showed strongly elevated nonsense-mediated messenger RNA decay–related transcripts in these *HAX1* mutant HPCs, but not in the *ELANE* mutant subtypes (supplemental Figure 3B; data not shown). In line with the fact that loss of HAX1 results in mitochondrial leakage,[3] MitoTracker Red CM-H2XRos and TMRM stainings showed reduced mitochondrial membrane potential in *HAX1* mutant HPCs (supplemental Figure 3C). Surprisingly, no upregulation of transcripts linked to the canonical unfolded protein response (UPR) pathway in *ELANE*-I60F HPCs was seen, as would be predicted from a mutation leading to protein misfolding (supplemental Figure 3D-E). Transcriptome analysis on more mature myeloid cells derived from these HPCs, by culturing the cells in the presence of CSF3, did not show upregulation of classical UPR-related genes and pathways (supplemental Figure 3F-H). Because PML-NBs have also been shown to control degradation of misfolded proteins, independent of the canonical UPR,[18] these data suggest that a PML-dependent mechanism, rather than the classical UPR, controlled levels of misfolded NE in the *ELANE*-I60F HPCs.
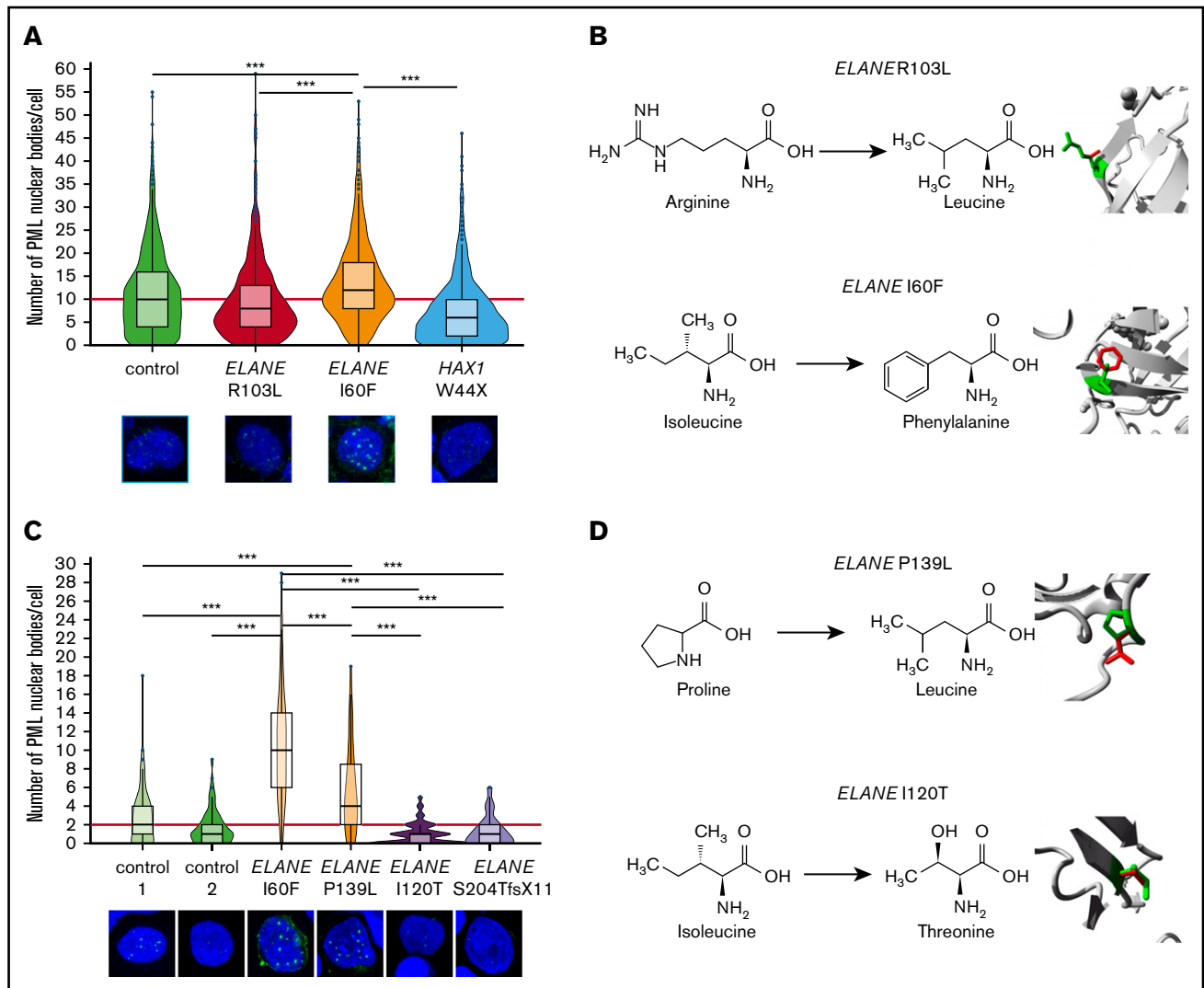
Figure 2. Increased numbers of PML-NBs in *ELANE*-SCN HPCs with predicted NE-misfolding mutations. (A) Quantifications of the number of PML-NBs per cell, by immunofluorescence stainings, shows increased numbers of PML-NBs in *ELANE*-I60F derived HPCs (data are pooled from 2 independent clones, 5 independent experiments, and 2 different stainings resulting in control, n = 1119; *ELANE*-R103L, n = 720; *ELANE*-I60F, n = 732; *HAX1*-W44X, n = 914, where n = the number of cells). The red line indicates the median number of PML-NBs/cell for the control HPCs. (B) Amino acid alterations of the *ELANE*-R103L and *ELANE*-I60F mutations, with a closeup of the mutation in ribbon-presentation. The wild-type amino acid is depicted in green and the mutant in red. (C) Quantifications of the number of PML-NBs in CD34+ bone marrow cells, showing increased numbers of PML-NBs in *ELANE*-mutant HPCs with predicted NE misfolding (I60F and P139L). The red line indicates the median number of PML-NBs/cell for the control HPCs. Cells analyzed: control 1, n = 89; control 2, n = 127; *ELANE*-I60F, n = 79; *ELANE*-P139L, n = 63; *ELANE*-I120T, n = 103; and *ELANE*-S204TfsX11 n = 74. (D) Amino acid alterations of the *ELANE*-P139L and *ELANE*-I120T mutations, depicted as outlined under panel B. ***$P < .001$.

PML activates metabolic pathways in *ELANE*-I60F HPCs

To assess which additional intracellular processes are controlled by PML, we compared the transcriptomes from HPCs generated from PML-proficient and PML-deficient *ELANE*-I60F and control iPSC lines. Deletion of PML reduced MYC and mTORC1-induced transcription in HPCs from *ELANE*-I60F, but not control HPCs, suggesting that PML drives metabolic pathways in these *ELANE* mutant HPCs (Figure 4A). Oxygen consumption assays showed that PML enhanced basal and maximal respiration as well as adenosine triphosphate (ATP) production in *ELANE*-I60F, which was not seen in control HPCs (Figure 4B). In addition, transcriptional

signatures indicated that PML activated cell cycling of *ELANE*-I60F HPCs, which translated into a moderately elevated fraction of cells in S-phase, whereas this was not seen in control HPCs (supplemental Figure 4A-B).

PML induces expression of *ELANE*-I60F

Transcriptome analysis further showed that *ELANE* was highly expressed in *ELANE*-I60F HPCs, relative to controls, whereas this increase in transcript levels was not observed in *ELANE*-R103L and *HAX1*-W44X HPCs (Figure 5A). Both wild-type and mutant transcripts could be detected in an approximately equal ratio in *ELANE*-I60F HPCs (supplemental Figure 5A). PML knockout
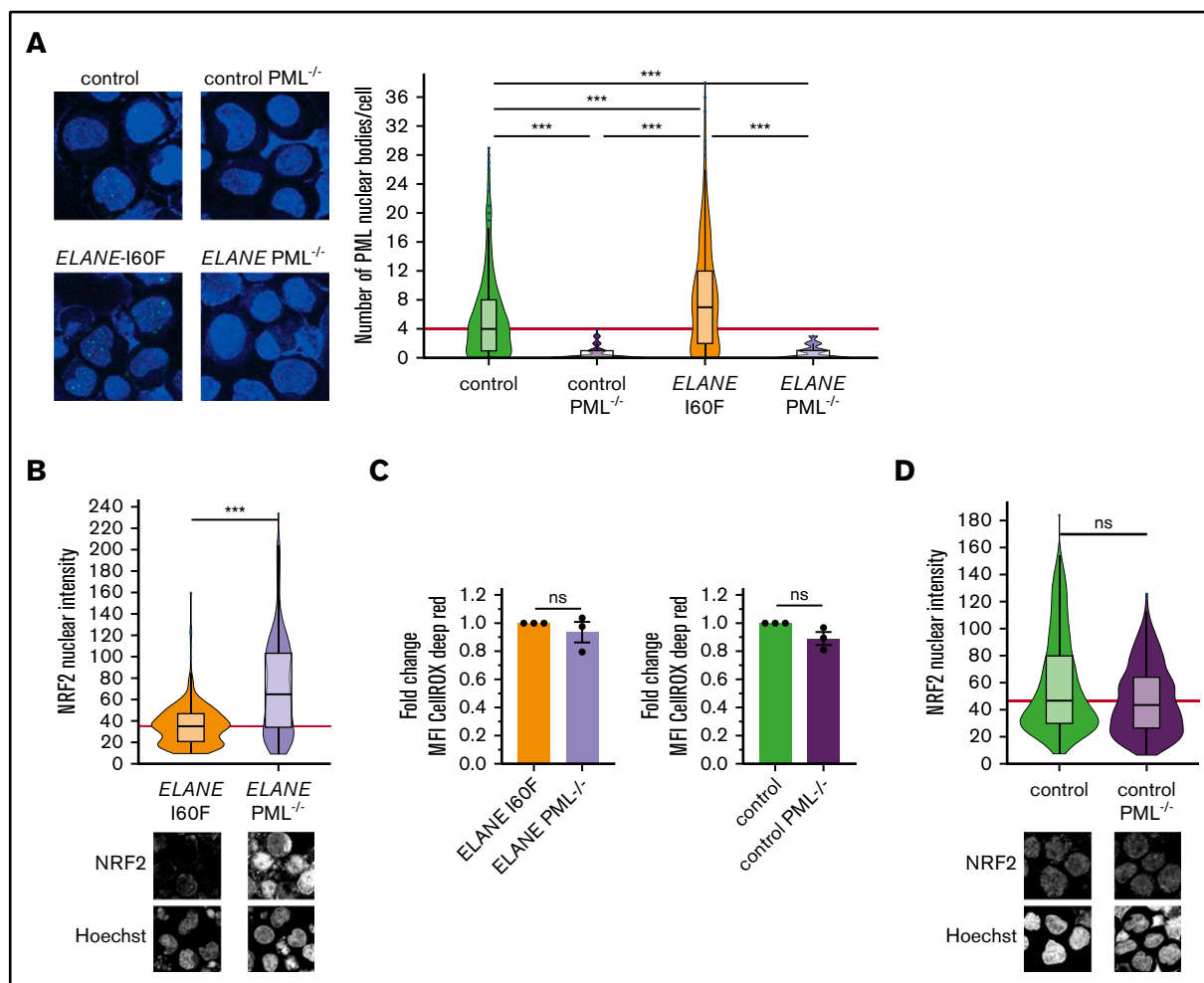
Figure 3. PML acts as a ROS sensor in *ELANE*-I60F HPCs. (A) Representative immunofluorescent image showing complete loss of PML-NBs after introduction of a stop codon in exon 3 of the PML gene and subsequent PML-NB quantification. The red line indicates the median number of PML-NBs/cell for the control HPCs. Number of cells analyzed (n): control, n = 441; control PML$^{-/-}$, n = 175; *ELANE*-I60F, n = 353; *ELANE*-I60F PML$^{-/-}$, n = 172. (B,D) Quantifications of immunofluorescent images showing increased nuclear NRF2 levels in *ELANE*-I60F PML-deficient HPCs (B), but not in control (D). Data are pooled from 3 independent experiments (*ELANE*-I60F, n = 365; *ELANE*(-I60F) PML$^{-/-}$, n = 370; control, n = 631; control PML$^{-/-}$, n = 644, where n = the number of cells). The red line indicates the median number of NRF2 nuclear intensity for the PML-proficient HPCs. Microscope settings (laser power) differed between figures. (C) Relative quantification of the mean fluorescent intensity (MFI) showing no increased CellROX Deep Red levels after PML knockout, where PML-proficient cells (*ELANE*-I60F or control) were used as baseline. Data are from 3 independent experiments. ***$P < .001$.

significantly reduced transcription of both the normal and mutant alleles in the *ELANE*-I60F HPCs (Figure 5B; supplemental Figure 5A), implying that PML drives the expression of *ELANE*-I60F and thereby exacerbates the disease phenotype. Extending this observation to protein levels, NE was detected at significantly higher levels in *ELANE*-I60F HPCs cells compared with control (Figure 5C). In both *ELANE*-I60F and control PML$^{-/-}$ HPCs, NE levels were strongly reduced, thus confirming the critical role of PML in *ELANE* expression in HPCs (Figure 5C). To exclude that this was a unique feature of the *ELANE*-I60F mutation in iPSC-derived HPCs, we analyzed NE expression in the CD34$^+$ HPCs from the primary BM samples shown in Figure 2C. In addition to the elevated formation of PML-NBs, NE protein levels were higher in the HPCs from patients with SCN with the NE-misfolding mutations (I60F and P139L) than in those from patients with other *ELANE* mutations or control HPCs (Figure 5D).

Correction of the *ELANE*-I60F mutation reverses the PML-mediated phenotype

To exclude that the increased formation of PML-NBs and higher expression of NE resulted from variations between the iPSC lines related to, for example, reprogramming or differences in (epi) genetic states of the lines, we corrected the *ELANE*-I60F mutation by CRISPR-Cas9 mediated genome editing in a fully isogenic setting (supplemental Figure 6). Immunofluorescent stainings showed that the numbers of PML-NBs in the corrected HPCs returned to basal levels (Figure 5E). Similarly, immunoblot analysis of 2 independent corrected clones showed that the increased NE levels in *ELANE*-I60F HPCs were reduced to control levels in corrected HPCs (Figure 5F). In line with PML-induced expression of metabolic and cell cycle–related pathways, GSEA showed significantly reduced expression of MYC targets, mTORC1
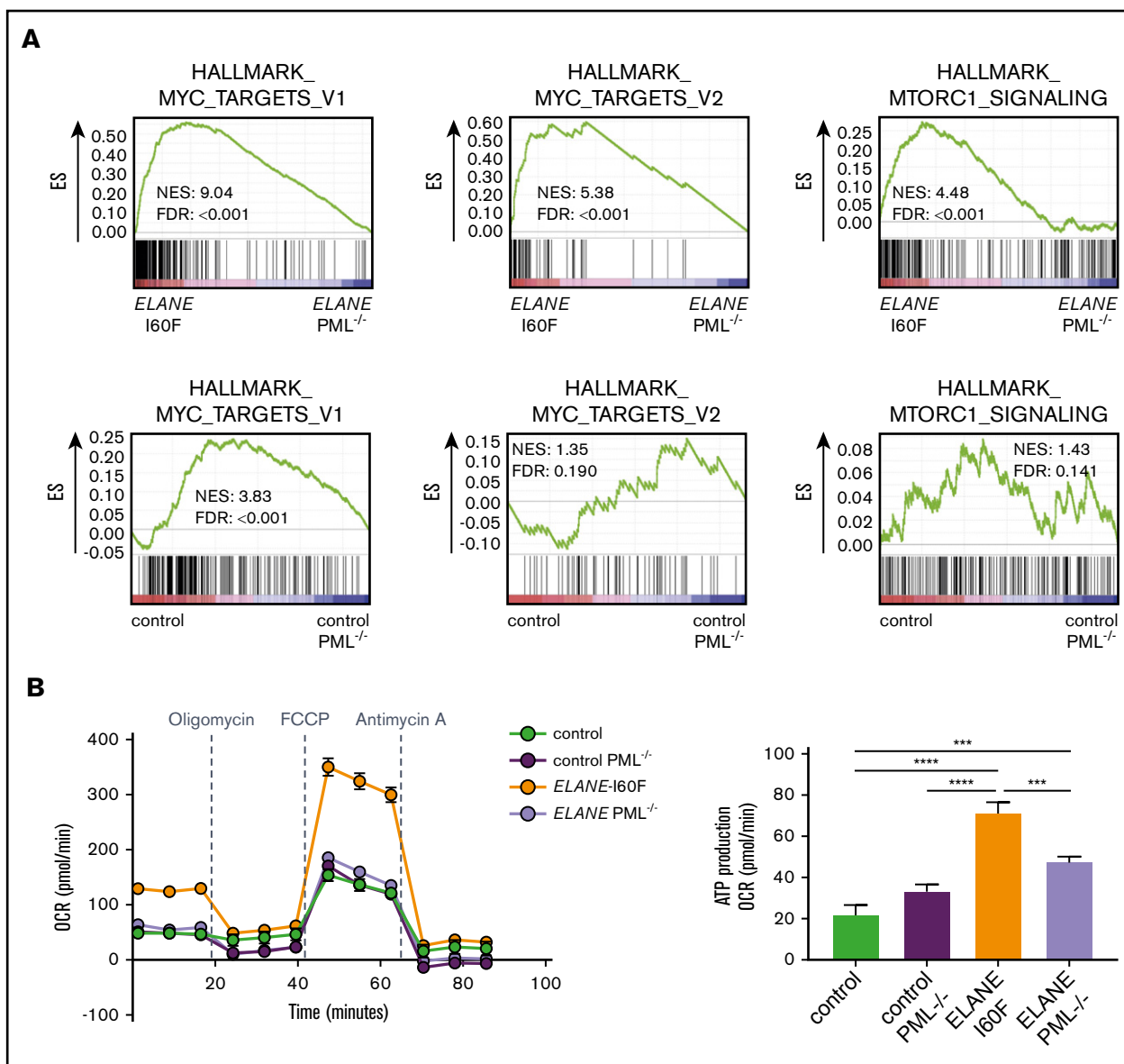
Figure 4. PML activates metabolic pathways in _ELANE_-I60F HPCs. (A) GSEA comparing PML proficient and deficient cells showing that PML induces MYC and mTORC1 signaling in _ELANE_-I60F, but not in control HPCs. Data are derived from 3 independent experiments. (B) Oxygen consumption rate (OCR) measured with the Seahorse mitochondrial stress test (Agilent) showing PML-dependent increases in basal respiration, ATP, and maximum respiration in _ELANE_-I60F cells (n = 5). FDR, false discovery rate; NES, normalized enrichment score. ***$P < .001$, ****$P < .0001$.

signaling, E2F targets, and G2M checkpoint in _ELANE_-I60F corrected lines (Figure 5G). These data establish that the increase in PML-NB formation, NE expression, and metabolic/cell cycle–related transcripts in _ELANE_-I60F HPCs were solely caused by the I60F amino acid alteration.

PML inhibits the CSF3 response of _ELANE_-I60F myeloid progenitors

The patient with SCN from whom the _ELANE_-I60F iPSC line was derived showed a poor clinical response to CSF3, where treatment with an excessive dosage of 60 to 70 µg/kg CSF3 resulted in only a modest increase in mature granulocytes. This was confirmed in granulocyte colony-forming unit (CFU-G) colony assays with titrated dosages of CSF3, showing that, although BM cells from the patient with _HAX1_-W44X SCN and 2 healthy controls show a dosage dependent increase in colony formation, the _ELANE_-I60F CFUs did not respond to CSF3 dosages exceeding 100 ng/mL (Figure 6A). Notably, colony formation in the presence of a myeloid cytokine cocktail consisting of IL-3, granulocyte-macrophage colony-stimulating factor, and CSF3 was within the normal range (ie, 127 colonies per 10^5 Ficoll-purified BM cells plated, where the normal reference of control BM cells in our laboratory is between 90 and 800 colonies per 10^5 cells). Thus, the lack of CSF3 response was not caused by a loss of myeloid progenitors per se. Similar CSF3 titration experiments showed that _ELANE_-I60F iPSC-derived
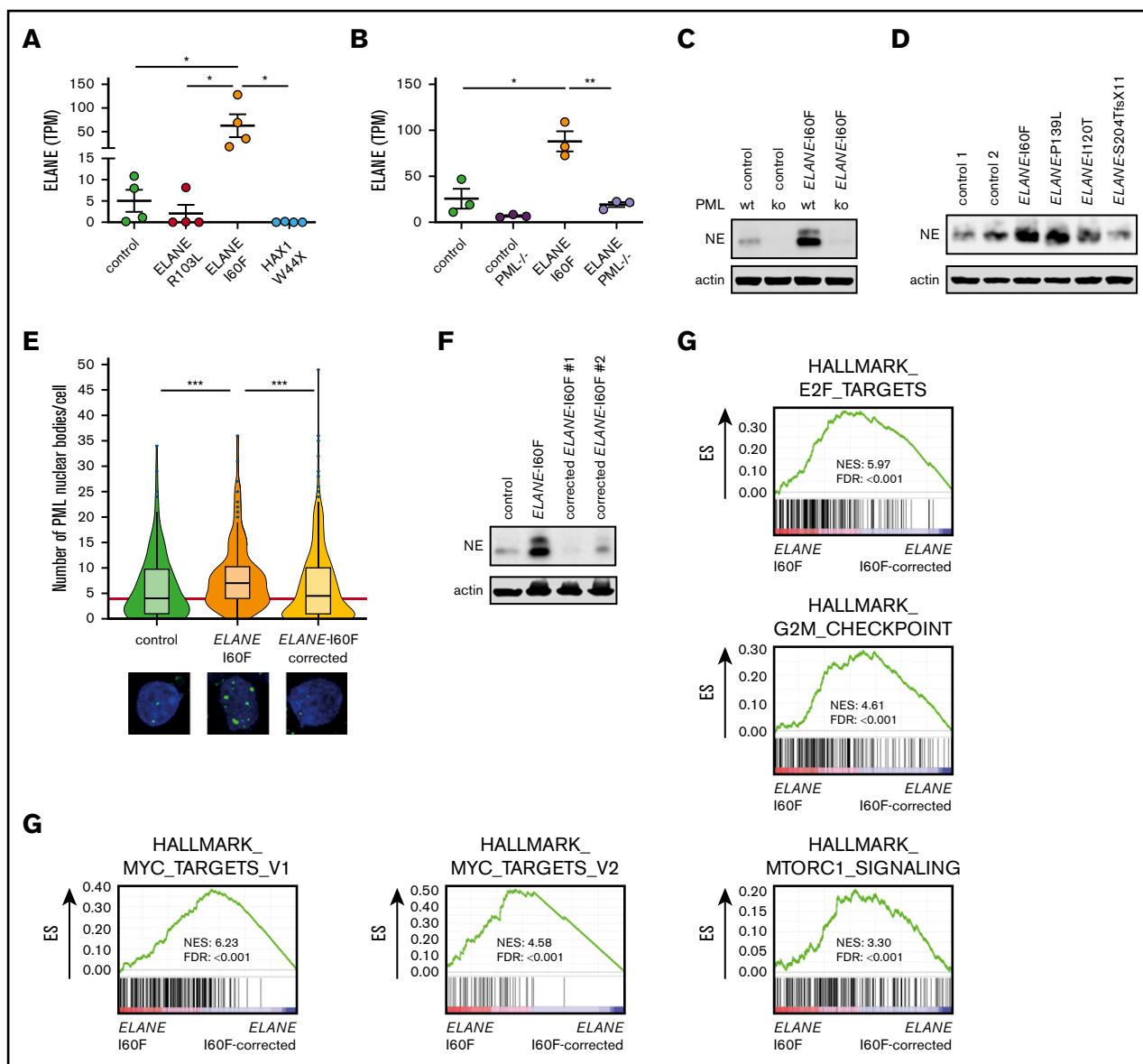
Figure 5. PML induces expression of *ELANE*-I60F. (A-B) Expression of ELANE in TPM showing upregulated expression in *ELANE*-I60F, but not *ELANE*-R103L and *HAX1*-W44X (data are derived from 2 independent clones and 2 independent experiments) (A), and increased levels of *ELANE* messenger RNA in *ELANE*-I60F HPCs, which is reduced to control levels when PML is absent (n = 3 independent experiments) (B). (C) Immunoblot showing PML-dependent NE protein abundance, with increased levels in *ELANE*-I60F cells. (D) Immunoblot of patient BM cells showing increased NE protein abundance in *ELANE*-mutant cells with predicted NE misfolding (I60F and P139L), but not others (I120T and S204TfsX11). (E) Quantification of immunofluorescence images showing increased, *ELANE*-I60F−driven numbers of PML-NBs. Data are pooled from 3 independent experiments and 3 independent *ELANE*-I60F−corrected clones resulting in; control: n = 126; *ELANE*-I60F: n = 144; *ELANE*-I60F corrected n = 442, where n = the number of cells. The red line indicates the median number of PML-NBs/cell for the control HPCs. (F) Immunoblot showing increased NE protein abundance in *ELANE*-I60F cells, which is reduced to control levels upon correction of the mutation, as shown in 2 independent clones. (G) GSEA comparing *ELANE*-I60F HPCs with corrected *ELANE*-I60F HPCs (2 independent experiments and 3 independent corrected clones) showing increased MYC, mTORC1, and cell cycle−related signatures in *ELANE*-I60F HPCs. *ELANE* PML$^{-/-}$, *ELANE*-I60F PML$^{-/-}$. *P < .05, **P < .01, ***P < .001.

HPCs were hyporesponsive to increasing dosages of CSF3 in CFU-G assays, which was restored after correction of the mutation (Figure 6B). A comparable restoration of the CSF3 response was seen in PML-deficient *ELANE*-I60F HPCs. Flow cytometric analysis of CD11b expression, a marker for myeloid differentiation, showed that *ELANE*-I60F HPCs produced significantly less CD11b$^+$ cells relative to control, upon switching to CSF3-containing suspension cultures, consistent with a reduced response to CSF3. In agreement

with the inhibitory effects of PML seen in colony assays, PML deletion almost completely restored the percentage of cells expressing CD11b (Figure 6C, left). Additionally, although significantly increased numbers of CD117$^+$ immature myeloid cells (myeloblasts/promyelocytes) remained present in the *ELANE*-I60F cultures compared with control cells, this fraction decreased upon deletion of PML (Figure 6C, right). Corroborating these findings, cytologic analysis showed that *ELANE* PML$^{-/-}$ and *ELANE*-I60F
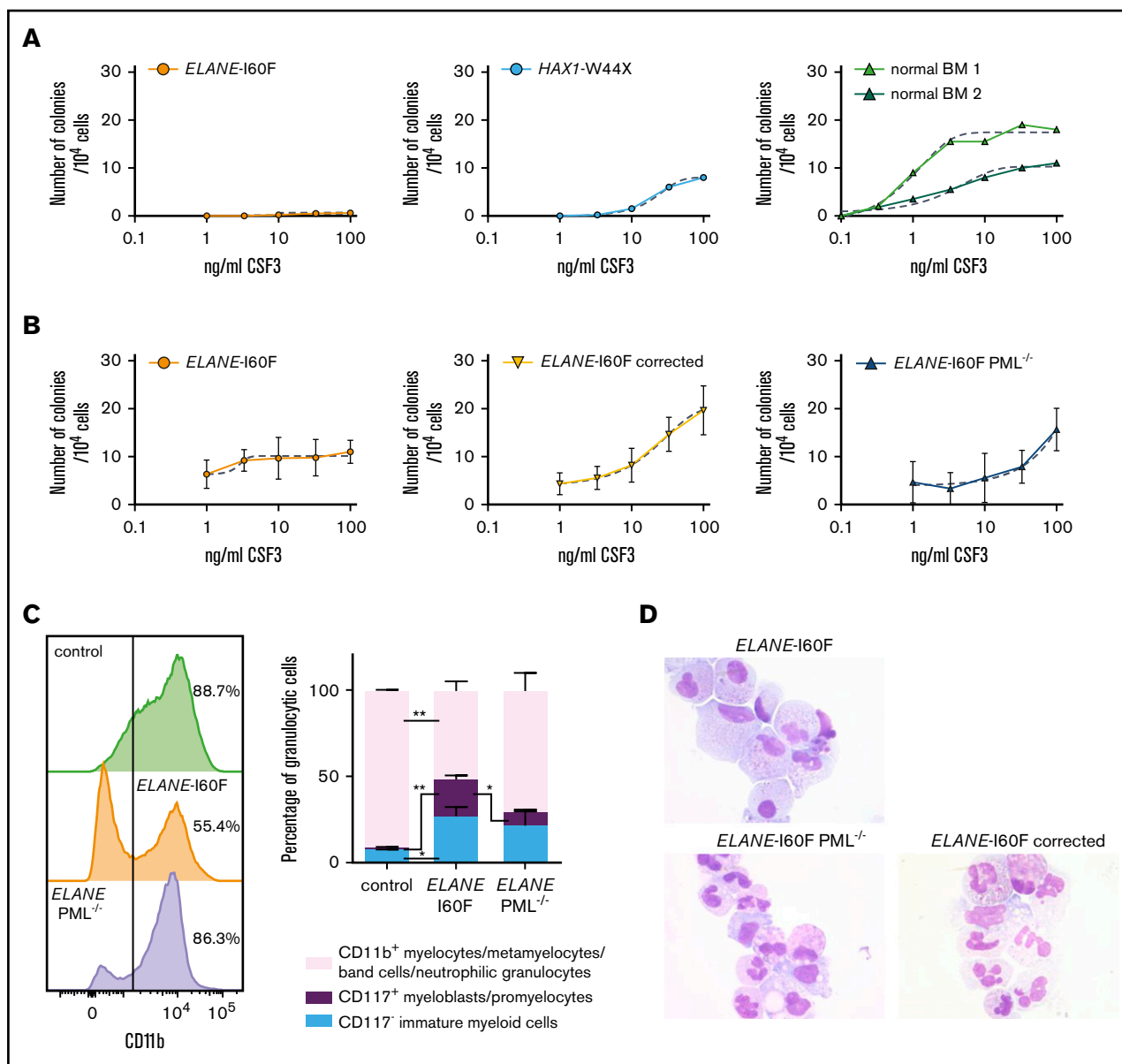
Figure 6. PML inhibits the CSF3 response of *ELANE*-I60F HPCs. (A) CFU-G assays on *ELANE*-I60F bone marrow cells showing a very limited CSF3 response with increasing dosages of CSF3, where *HAX1*-W44X and normal bone marrow cells show a CSF3-induced increase in colony formation. (B) CFU-G assays on iPSC-derived HPCs showing a similar hyporesponsiveness in *ELANE*-I60F cells, which is restored upon correction of the mutation and partly restored by the removal of PML (data are pooled from 3 independent experiments performed in triplicate). Dashed line indicates a nonlinear fitted curve. (C) Representative FACS histogram depicting CD11b expression (left) and subsequent quantifications of the myeloid cells present in CSF3-containing liquid culture (right; n = 3) showing an elevated ratio of immature vs mature myeloid cells in *ELANE*-I60F cells relative to controls, which was partly reverted to normal after PML knockout (*ELANE* PML$^{-/-}$, *ELANE*-I60F PML$^{-/-}$). *P < .05, **P < .01. (D) Representative May Grünwald-Giemsa–stained images of parental, PML-deficient, and corrected *ELANE*-I60F cells.

gene-corrected cells differentiated toward mature neutrophils in these cultures, whereas *ELANE*-I60F cells mainly accumulated in more immature stages of myeloid differentiation (Figure 6D). Taken together, these data imply that PML contributes to the poor CSF3 response and decreased neutrophil differentiation seen in this patient with SCN.

Discussion

By generating iPSC models, we addressed how CD34$^+$CD45$^+$ HPCs from patients with SCN are affected by mutations in

ELANE or *HAX1*, with emphasis on the levels of oxidative stress. We showed that, although elevated ROS levels and activation of the NRF2 antioxidant pathway were detectable in all cases tested, increased PML-NB formation was seen in a subgroup of *ELANE*-SCN patients with mutations leading to NE protein misfolding. Elevated PML-NB formation is a characteristic of cells undergoing acute and more excessive oxidative stress than cells under more physiological conditions.[19] The focus of this study was to unravel the function of PML in these cases.
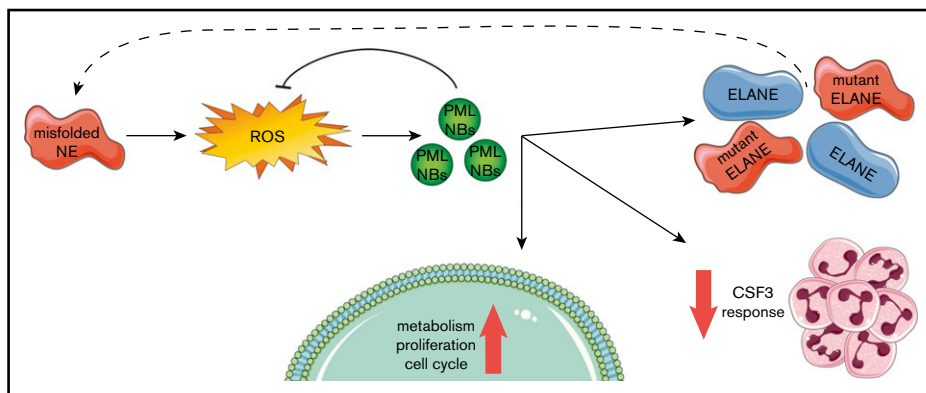
Figure 7. Graphical representation of the PML-mediated responses in *ELANE*-I60F HPCs. *ELANE* mutations with predicted NE misfolding result in excessive doses of ROS, inducing the formation of PML-NBs. PML-NBs are important for reducing ROS levels, while also inducing metabolism, proliferation, and cell cycling. In addition, PML reduces the response to CSF3 and induces the transcription of (mutant) *ELANE*, providing a feed-forward mechanism.

Previous studies have shown that *ELANE* mutations evoke "classical" UPR responses in both mouse and human SCN models, likely caused by NE misfolding.[11,36] However, in a more recent study, mutant *ELANE* failed to induce an UPR, even though the mutation predicted NE misfolding.[37] A possible explanation for this discrepancy is that the wide spectrum of *ELANE*-mutations in patients with SCN differentially affect NE protein structure and folding.[9,10] It is therefore not inconceivable that different structural changes might result in variable degrees of NE misfolding and consequently activate different (ie, canonical vs PML-mediated, UPR responses).

Our findings fit into a model (Figure 7) in which *ELANE* mutations that result in NE protein misfolding (eg, by insertion of a bulky amino acid in the core of the protein) induce an increased level of oxidative stress in CD34$^+$CD45$^+$ HPCs. As a consequence, PML-NBs are being formed, which not only act to reduce excessive ROS levels, but also stimulate metabolism and, to a lesser extent, proliferation of the HPCs. In addition, PML dampened the CSF3 responsiveness of *ELANE*-I60F HPCs in vitro, providing a possible explanation for the ineffective clinical CSF3 response in this patient. Finally, transcription of (mutant) *ELANE* and NE protein expression strongly depended on PML, suggestive of a PML-driven feed-forward loop aggravating the consequences of the NE misfolding mutation.

Even though a confirmation of the *ELANE*-I60F iPSC-derived data were obtained in primary CD34$^+$ cells from this patient with SCN, as well as in a patient with SCN with another predicted misfolding mutation (*ELANE*-P139L), it still needs to be addressed to what extent cases of SCN with NE misfolding mutations other than *ELANE*-I60F and *ELANE*-P139L fit into the model shown in Figure 7. Keeping in mind that a large number of different *ELANE* mutations have been reported in both SCN and cyclic neutropenia (CyN), some of which overlap between the 2 conditions,[9] additional unknown host factors must have an impact on disease characteristics, such as determining (1) cyclic vs severe neutropenia, (2) risk of leukemic transformation, and (3) response to CSF3 treatment and variations in doses.

Despite these limitations, we propose that SCN cases in which CD34$^+$ cells accumulate increased numbers of PML-NBs because of specific *ELANE* mutations predicting NE-misfolding represent a distinct subgroup of patients with specific clinical features. First of all, as increased ROS levels lead to more severe oxidative damage, these patients may face a higher risk to develop MDS or AML than patients with lower levels of oxidative stress in their HPCs. This is in line with the fact that patients with SCN who do not respond well to CSF3 treatment have a much higher chance to progress to MDS or AML than good responders.[5,6,38]

The finding that PML enhanced MYC and mTORC1 signaling in *ELANE*-I60F HPCs, leading to increased metabolic and proliferative activity, supports the notion of increased potential for progression to leukemia.[39,40] This appears in contrast with earlier studies showing that PML represses the AKT/mTOR pathway under hypoxic conditions in, for example, models of neoangiogenesis.[41,42] Potential explanations for this discrepancy might relate to the fact that PML functions can be divergent depending on the oxidative state of cells (ie, hypoxic vs hyperoxic) or depend on the cell type or developmental stage of cells. In line with this, although PML has well-documented tumor suppressive functions, more recent evidence suggests that, depending on the cellular context, PML also has oncogenic properties.[43,44] Further studies are needed to resolve this issue and also to elucidate how PML and upregulation of mTORC1 signaling are transcriptionally connected.

Finally, the observation that expression of NE levels in the *ELANE*-I60F HPCs strongly depended on PML is intriguing. RNA-sequencing data indicated that transcription of both wild-type and mutant *ELANE* alleles fully depended on the presence of PML. PML chromatin immunoprecipitation sequencing data from the PML-RARα zinc-inducible U937 cell line (UPR9) showed that PML binds to the promoter/enhancer region of *ELANE*,[45] which could suggest that PML directly controls its transcription. Although suggestive of a PML-mediated feed-forward loop as illustrated by the dashed arrow in Figure 7, the possibility that mutant NE is, at least partly, degraded by a PML-driven mechanism should be taken into account, similar to the mechanism shown in a model of neurodegeneration.[18]

In summary, this study sheds further light on the complex and heterogeneous natural history of SCN and identified a subset of patients with *ELANE*-SCN characterized by the activation of PML-mediated responses of hematopoietic progenitors, which may ultimately help to design new strategies for disease management for these cases.

Acknowledgments

Authorship

References

1. Skokowa J, Dale DC, Touw IP, Zeidler C, Welte K. Severe congenital neutropenias. *Nat Rev Dis Primers*. 2017;3(1):17032.

2. Dale DC, Person RE, Bolyard AA, et al. Mutations in the gene encoding neutrophil elastase in congenital and cyclic neutropenia. *Blood*. 2000;96(7):2317-2322.

3. Klein C, Grudzien M, Appaswamy G, et al. HAX1 deficiency causes autosomal recessive severe congenital neutropenia (Kostmann disease). *Nat Genet*. 2007;39(1):86-92.

4. Dale DC, Bonilla MA, Davis MW, et al. A randomized controlled phase III trial of recombinant human granulocyte colony-stimulating factor (filgrastim) for treatment of severe chronic neutropenia. *Blood*. 1993;81(10):2496-2502.

5. Rosenberg PS, Alter BP, Bolyard AA, et al; Severe Chronic Neutropenia International Registry. The incidence of leukemia and mortality from sepsis in patients with severe congenital neutropenia receiving long-term G-CSF therapy. *Blood*. 2006;107(12):4628-4635.

6. Rosenberg PS, Zeidler C, Bolyard AA, et al. Stable long-term risk of leukaemia in patients with severe congenital neutropenia maintained on G-CSF therapy. *Br J Haematol*. 2010;150(2):196-199.

7. Glaubach T, Minella AC, Corey SJ. Cellular stress pathways in pediatric bone marrow failure syndromes: many roads lead to neutropenia. *Pediatr Res*. 2014;75(1-2):189-195.

8. Grenda DS, Johnson SE, Mayer JR, et al. Mice expressing a neutrophil elastase mutation derived from patients with severe congenital neutropenia have normal granulopoiesis. *Blood*. 2002;100(9):3221-3228.

9. Germeshausen M, Deerberg S, Peter Y, Reimer C, Kratz CP, Ballmaier M. The spectrum of ELANE mutations and their implications in severe congenital and cyclic neutropenia. *Hum Mutat*. 2013;34(6):905-914.

10. Horwitz MS, Duan Z, Korkmaz B, Lee HH, Mealiffe ME, Salipante SJ. Neutrophil elastase in cyclic and severe congenital neutropenia. *Blood*. 2007;109(5):1817-1824.

11. Köllner I, Sodeik B, Schreek S, et al. Mutations in neutrophil elastase causing congenital neutropenia lead to cytoplasmic protein accumulation and induction of the unfolded protein response. *Blood*. 2006;108(2):493-500.

12. Bernardi R, Pandolfi PP. Structure, dynamics and functions of promyelocytic leukaemia nuclear bodies. *Nat Rev Mol Cell Biol*. 2007;8(12):1006-1016.

13. Chang HR, Munkhjargal A, Kim MJ, et al. The functional roles of PML nuclear bodies in genome maintenance. *Mutat Res*. 2018;809:99-107.

14. Maarifi G, Chelbi-Alix MK, Nisole S. PML control of cytokine signaling. *Cytokine Growth Factor Rev*. 2014;25(5):551-561.

15. Niwa-Kawakita M, Wu HC, Thé H, Lallemand-Breitenbach V. PML nuclear bodies, membrane-less domains acting as ROS sensors? *Semin Cell Dev Biol*. 2018;80:29-34.

16. Sahin U, de Thé H, Lallemand-Breitenbach V. PML nuclear bodies: assembly and oxidative stress-sensitive sumoylation. *Nucleus*. 2014;5(6):499-507.

17. Tessier S, Martin-Martin N, de Thé H, Carracedo A, Lallemand-Breitenbach V. Promyelocytic leukemia protein, a protein at the crossroad of oxidative stress and metabolism. *Antioxid Redox Signal*. 2017;26(9):432-444.

18. Guo L, Giasson BI, Glavis-Bloom A, et al. A cellular system that degrades misfolded proteins and protects against neurodegeneration. *Mol Cell*. 2014;55(1):15-30.

19. Niwa-Kawakita M, Ferhi O, Soilihi H, Le Bras M, Lallemand-Breitenbach V, de Thé H. PML is a ROS sensor activating p53 upon oxidative stress. *J Exp Med*. 2017;214(11):3197-3206.

20. Warlich E, Kuehle J, Cantz T, et al. Lentiviral vector design and imaging approaches to visualize the early stages of cellular reprogramming. *Mol Ther*. 2011;19(4):782-789.

21. Nayak RC, Trump LR, Aronow BJ, et al. Pathogenesis of ELANE-mutant severe neutropenia revealed by induced pluripotent stem cells. *J Clin Invest*. 2015;125(8):3103-3116.

22. van Dongen JJ, Lhermitte L, Böttcher S, et al; EuroFlow Consortium (EU-FP6, LSHB-CT-2006-018708). EuroFlow antibody panels for standardized n-dimensional flow cytometric immunophenotyping of normal, reactive and malignant leukocytes. *Leukemia*. 2012;26(9):1908-1975.

23. Olofsen PA, Touw IP. Modeling severe congenital neutropenia in induced pluripotent stem cells. In: Birbrair A, ed. Recent Advances in iPSC Disease Modeling, vol. 1. Chapter 5. Waltham, MA: Academic Press; 2020:85-101

24. Schindelin J, Arganda-Carreras I, Frise E, et al. Fiji: an open-source platform for biological-image analysis. *Nat Methods*. 2012;9(7):676-682.

25. Dobin A, Davis CA, Schlesinger F, et al. STAR: ultrafast universal RNA-seq aligner. *Bioinformatics*. 2013;29(1):15-21.

26. Trapnell C, Williams BA, Pertea G, et al. Transcript assembly and quantification by RNA-Seq reveals unannotated transcripts and isoform switching during cell differentiation. *Nat Biotechnol*. 2010;28(5):511-515.

27. Anders S, Pyl PT, Huber W. HTSeq–a Python framework to work with high-throughput sequencing data. *Bioinformatics*. 2015;31(2):166-169.

28. Love MI, Huber W, Anders S. Moderated estimation of fold change and dispersion for RNA-seq data with DESeq2. *Genome Biol*. 2014;15(12):550.

29. Mootha VK, Lindgren CM, Eriksson KF, et al. PGC-1alpha-responsive genes involved in oxidative phosphorylation are coordinately downregulated in human diabetes. *Nat Genet*. 2003;34(3):267-273.

30. Subramanian A, Tamayo P, Mootha VK, et al. Gene set enrichment analysis: a knowledge-based approach for interpreting genome-wide expression profiles. *Proc Natl Acad Sci USA*. 2005;102(43):15545-15550.

31. Pertea M, Kim D, Pertea GM, Leek JT, Salzberg SL. Transcript-level expression analysis of RNA-seq experiments with HISAT, StringTie and Ballgown. *Nat Protoc*. 2016;11(9):1650-1667.

32. Xia J, Link DC. Severe congenital neutropenia and the unfolded protein response. *Curr Opin Hematol*. 2008;15(1):1-7.

33. Ishii T, Itoh K, Takahashi S, et al. Transcription factor Nrf2 coordinately regulates a group of oxidative stress-inducible genes in macrophages. *J Biol Chem*. 2000;275(21):16023-16029.

34. Venselaar H, Te Beek TA, Kuipers RK, Hekkelman ML, Vriend G. Protein structure analysis of mutations causing inheritable diseases. An e-Science approach with life scientist friendly interfaces. *BMC Bioinformatics*. 2010;11(1):548.

35. Nagy E, Maquat LE. A rule for termination-codon position within intron-containing genes: when nonsense affects RNA abundance. *Trends Biochem Sci*. 1998;23(6):198-199.

36. Grenda DS, Murakami M, Ghatak J, et al. Mutations of the ELA2 gene found in patients with severe congenital neutropenia induce the unfolded protein response and cellular apoptosis. *Blood*. 2007;110(13):4179-4187.

37. Garg B, Mehta HM, Wang B, Kamel R, Horwitz MS, Corey SJ. Inducible expression of a disease-associated *ELANE* mutation impairs granulocytic differentiation, without eliciting an unfolded protein response. *J Biol Chem*. 2020;295(21):7492-7500.

38. Cross CE, Halliwell B, Borish ET, et al. Oxygen radicals and human disease. *Ann Intern Med*. 1987;107(4):526-545.

39. Ben-Sahra I, Manning BD. mTORC1 signaling and the metabolic control of cell growth. *Curr Opin Cell Biol*. 2017;45:72-82.

40. Stine ZE, Walton ZE, Altman BJ, Hsieh AL, Dang CV. MYC, metabolism, and cancer. *Cancer Discov*. 2015;5(10):1024-1039.

41. Trotman LC, Alimonti A, Scaglioni PP, Koutcher JA, Cordon-Cardo C, Pandolfi PP. Identification of a tumour suppressor network opposing nuclear Akt function. *Nature*. 2006;441(7092):523-527.

42. Bernardi R, Guernah I, Jin D, et al. PML inhibits HIF-1alpha translation and neoangiogenesis through repression of mTOR. *Nature*. 2006;442(7104):779-785.

43. Mazza M, Pelicci PG. Is PML a tumor suppressor? *Front Oncol*. 2013;3:174.

44. Chung YL, Wu ML. Dual oncogenic and tumor suppressor roles of the promyelocytic leukemia gene in hepatocarcinogenesis associated with hepatitis B virus surface antigen. *Oncotarget*. 2016;7(19):28393-28407.

45. Martens JH, Brinkman AB, Simmer F, et al. PML-RARalpha/RXR alters the epigenetic landscape in acute promyelocytic leukemia. *Cancer Cell*. 2010;17(2):173-185.